I.V. PYLYUK, O.A. DOBUSH, M.P. KOZLOVSKII, R.V. ROMANIK, M.A. SHPOT

Yukhnovskii Institute for Condensed Matter Physics of the Nat. Acad. of Sci. of Ukraine
(1 Svientsitskii Street, Lviv 79011; e-mail: piv@icmp.lviv.ua, dobush@icmp.lviv.ua,
mpk@icmp.lviv.ua, romanik@icmp.lviv.ua, shpot.mykola@gmail.com)

INFLUENCE OF ATTRACTIVE PARTS OF INTERACTION POTENTIALS ON CRITICAL POINT PARAMETERS

We will investigate how microscopic features of interparticle potentials influence the macroscopic critical point parameters. Our analytic calculations are based on the cell model for continuous many-particle systems. We will explore two types of pair interactions described by the Morse potential and a Curie–Weiss-type potential. For the Morse fluids, we present numerical results obtained with the microscopic parameters corresponding to the alkali metals sodium (Na) and potassium (K). The calculated dimensionless critical point parameters for liquid Na and K, expressed in dimensional units, allow for the direct comparison with available experimental and simulation data. For the Curie–Weiss cell model with competing interactions, which exhibits a sequence of first-order phase transitions, we examine the critical parameters for the first three critical points. We analyze our results by varying the attractive part of the Morse potential and the Curie–Weiss attraction strength, providing the insights into how these microscopic characteristics change the critical point coordinates.

K e y w o r d s: Morse potential, Curie–Weiss-type potential, attraction strength, critical point parameters, phase transitions.

1. Introduction

The study of critical behavior in many-particle systems, particularly the behavior of fluids near the liquid-gas critical point, remains one of the central themes in statistical physics [1–4]. Of particular interest is the problem of establishing a connections between microscopic characteristics of the interparticle interactions and macroscopic parameters of the critical point, such as temperature, density, and pressure. Studying this problem deepens our understanding of phase transitions and supports the development of effective models for real fluids. The influence of interactions receives considerable attention in the interpretation of experimental data. For example, the enhancement of solute-solvent interactions caused by the influence of ionic impurities (as, for example, the

NaCl salt) on aqueous solutions of organic molecules leads to an increase in the size of water-solute clusters and results in a reduction of the asymptotic critical region and a decrease in the critical viscosity amplitude [5].

Given the important role of the interparticle interactions in shaping the critical properties, it is reasonable to focus specifically on the attractive part of the potential, since changes in this component can influence the position of the critical point.

The aim of this work is to evaluate the influence of parameters of the attractive part of the potential on the critical point characteristics in a continuous model system. To this end, we consider both the classical Morse potential and the Curie–Weiss interaction potential. These potentials possess different functional forms of the attractive component. The Morse potential contains a term that describes exponential decay of the attractive interaction with distance. The Curie–Weiss potential is given by a global non-local attractive term of equal strength for any pair of particles.

The analysis of data for the short-range (Morse potential) and long-range (Curie–Weiss potential) at-

traction allows for a better understanding of the critical behavior pattern of systems with these two types of interaction. The analytic expressions used in numerical calculations and results are presented in Section 2 in the case of the Morse potential and, in Section 3, for the case of Curie–Weiss-type interaction. Conclusions are given in Section 4.

2. Critical Point Parameters for Morse Fluids

2.1. General scope

Our description of the critical behavior of fluids is carried out within the framework of the grand canonical ensemble (see, for example, [3]) based on the cell fluid model proposed in [6, 7].

We consider an open system of interacting particles in volume V partitioned into N_v cubic cells. Each cell has volume $v = V/N_v = c^3$, where c is its linear size.

The Morse interaction potential as a function of distance $r \equiv |\mathbf{r}_1 - \mathbf{r}_2|/R_0$ between particles with coordinates $\mathbf{r}_1$, $\mathbf{r}_2 \in \mathbb{R}^3$ has the form [8–10]

$$
\begin{aligned}
\tilde{U}(r) &= \Psi(r) - U(r), \\
\Psi(r) &= De^{-2(r-1)/\alpha_R}, \\
U(r) &= 2De^{-(r-1)/\alpha_R}.
\end{aligned}
\tag{1}
$$

Here, $\Psi(r)$ and $U(r)$ denote the repulsive and attractive parts of the potential, respectively, and $\alpha_R = \alpha/R_0$, where α is the effective interaction radius. The parameter R_0 corresponds to the minimum of the function $\tilde{U}(r)$, and D determines the depth of the potential well. We use R_0 as a reference length and measure the distances in units of R_0. Thus, the linear size of each cell c and its volume v are determined in units of R_0 and R_0^3, respectively.

In the renormalization group framework used in [9, 11], the critical temperature for fluids is determied from the equation

$$
\begin{aligned}
&1 + q + R^{(0)}\sqrt{u^*} - \tilde{a}_2 \beta_c W(0) - \\
&- R^{(0)} \frac{a_4}{\sqrt{u^*}}(\beta_c W(0))^2 = 0,
\end{aligned}
\tag{2}
$$

where $\beta_c = (k_{\mathrm{B}} T_c)^{-1}$ is the inverse critical temperature, k_{B} is the Boltzmann constant, T_c is the critical temperature. Further, $W(0)$ is the Fourier transform of the effective interaction potential at zero wave vector $\mathbf{k}$, and $\tilde{a}_2$, a_4 are coefficients in the initial expression for the grand partition function [9]. The quantity

q is related to averaging the square of the wave vector in the function $W(k)$. The value of $R^{(0)}$ is determined by the elements and smallest eigenvalue of the renormalization group linear transformation matrix, and u^* is the fixed-point coordinate.

At temperatures T below the critical one, the reduced density $\rho^* = (\langle N \rangle/V)R_0^3$, where $\langle N \rangle$ is the average number of particles in the system, and the effective chemical potential M are related via the following nonlinear equation [10]

$$
\rho^* = \frac{R_0^3}{v}\left[n_g - M + \sigma_{00}^{(-)}\left(\tilde{h}^2 + h_{cm}^2\right)^{\frac{d-2}{2(d+2)}}\right].
\tag{3}
$$

Note, that in [10], this equation was written in terms of $\bar{n} = \langle N \rangle/N_v$, which is related to ρ^* as $\bar{n} = \rho^* v/R_0^3$. The quantity $\tilde{h}$ is proportional to M, while h_{cm} is determined by the relative temperature $\tau = (T - T_c)/T_c$. The first term n_g on the right-hand side of (3) is determined by the coefficients of the initial expression for the grand partition function. The coefficient $\sigma_{00}^{(-)}$ of the third term depends on the quantity $\alpha_m = \tilde{h}/h_{cm}$ depending both on the physical chemical potential μ through M, and the relative temperature τ. The space dimension d is fixed at $d = 3$ in our current discussion.

The pressure P as a function of the temperature T and density $\bar{n}$ is given by the equation of state [9, 10]. For temperatures below T_c, it is given by

$$
\begin{aligned}
\frac{Pv}{k_{\mathrm{B}}T} &= P_a^{(-)}(T) + E_\mu + \left(\frac{\bar{n} - n_g}{\sigma_{00}^{(-)}}\right)^6 \times \\
&\times \left[e_0^{(-)}\frac{\alpha_m}{(1+\alpha_m^2)^{1/2}} + \gamma_s^{(-)} - e_2^{(-)}\right].
\end{aligned}
\tag{4}
$$

The quantity $P_a^{(-)}(T)$ contains an analytic temperature dependence. The coefficient $\gamma_s^{(-)}$ characterizes a nonanalytical contribution to the thermodynamic potential. The quantities $e_0^{(-)}$ and $e_2^{(-)}$, as well as $\sigma_{00}^{(-)}$, are related to the roots of the associated cubic equation. Explicit expressions for all these quantities, as well as for E_μ, are given in [10].

2.2. Numerical results

We employed the above microscopic description of critical behavior of the Morse fluid to compute the critical values for the reduced temperature T^*, the reduced density ρ^*, and the reduced pressure P^*. These

quantities are related to their dimensional counterparts via

$$\frac{k_{\mathrm{B}}T}{D} = T^*, \quad \rho\frac{N_{\mathrm{A}}R_0^3}{M_{\mathrm{mol}}} = \rho^*, \quad \frac{PR_0^3}{D} = P^*, \qquad (5)$$

where $k_{\mathrm{B}} = 1.380649\times10^{-23}\ \mathrm{J\cdot K^{-1}}$ is the Boltzmann constant, $N_{\mathrm{A}} = 6.02214076 \times 10^{23}\ \mathrm{mol^{-1}}$ is the Avogadro number, and M_{mol} is the molar mass. The critical temperature T_c^* is calculated using Eq. (2). The critical density ρ_c^* and critical pressure P_c^* are obtained from (3) and (4), respectively, at $M = 0$ and $T = T_c$.

We use the Morse interaction potential parameters characteristic for sodium (molar mass $M_{\mathrm{Na}} = 22.9898\ \mathrm{g\cdot mol^{-1}}$) and potassium (molar mass $M_{\mathrm{K}} = 39.0983\ \mathrm{g\cdot mol^{-1}}$). These specific parameters are [12, 14]: $R_0 = 5.3678$ Å, $D = 0.9241 \times 10^{-13}$ erg for Na, and $R_0 = 6.4130$ Å, $D = 0.8530 \times 10^{-13}$ erg for K. Our results for the critical point are

for Na:

$$T_c^* = 4.0277, \quad \rho_c^* v/R_0^3 = 0.9971, \quad P_c^* = 0.4735; \ (6)$$

for K:

$$T_c^* = 3.3043, \quad \rho_c^* v/R_0^3 = 0.9347, \quad P_c^* = 0.4075. \ (7)$$

To facilitate comparison with the results of other studies, such as computer simulation [12] and experiment [13], we transform our dimensionless quantities from (6) and (7) into dimensional ones employing the relations (5). Thus, we obtain numerical estimates of the critical point parameters for Na and K presented in Table 1. Note that the critical density in Table 1 for the cell fluid model is normalized to v/R_0^3.

2.3. Behavior of critical point parameters with changes in the width of the attractive part of the Morse potential

For potassium (K), the ratio $R_0/\alpha = 3.0564$ is somewhat larger than the analogous quantity $R_0/\alpha = 2.9544$ for sodium (Na) [12]. A larger R_0/α implies a smaller potential well width, meaning a narrower attractive part of the Morse potential.

From Table 1, we observe that both the critical temperature T_c and critical pressure P_c are smaller for K than for Na. This suggests that narrowing the attractive part of the Morse potential leads to smaller values of T_c and P_c. This conclusion aligns with the findings of [15], where liquid-vapor coexistence curves were computed using the NPT plus test

particle method for various interatomic model potentials, including Lennard–Jones, Morse, and modified Stillinger–Weber. Furthermore, our results indicate that the critical density ρ_c also decreases as the attractive part of the interaction potential narrows.

The critical temperature and pressure for liquid alkali metals sodium and potassium, derived using the approach developed in [9, 10] and presented in Table 1, show better agreement with experimental data [13] than the Monte Carlo results from [12]. This is consistent with the authors' note in [12] that their critical pressure results for Na and K (quoted in Table 1) deviate significantly from experimental values due to an overestimation of the critical temperature.

3. Critical Point Parameters for Fluid Systems with the Curie–Weiss Potential

Let us turn our attention to a one-component continuous system with Curie–Weiss-type interaction. We begin by presenting some basic formulas from [7] and [16] used in this investigation.

3.1. Key definitions and relations

The Curie–Weiss-type interaction potential is given by

$$\Phi_{N_v}(\mathbf{r}, \mathbf{r}') = -\frac{g_a}{N_v} + g_r \sum_{l=1}^{N_v} I_{\Delta_\ell}(\mathbf{r})I_{\Delta_\ell}(\mathbf{r}'), \qquad (8)$$

where

$$I_{\Delta_\ell}(\mathbf{r}) = \begin{cases} 1, & \mathbf{r} \in \Delta_\ell, \\ 0, & \mathbf{r} \notin \Delta_\ell \end{cases} \qquad (9)$$

is the indicator function of the cell Δ_ℓ, for $l = 1, ..., N_v$. As in Subsection 2.1, we consider a system of interacting particles in a volume V, which comprises N_v congruent cells, each of volume $v = c^3$. The

Table 1. **Critical temperature T_c, density ρ_c, and pressure P_c for sodium (Na) and potassium (K): cell fluid model (CFM) in the ρ^4 approximation vs Monte Carlo simulation and experimental results**

Research method	Na			K		
	T_c, K	ρ_c, kg/m³	P_c, bar	T_c, K	ρ_c, kg/m³	P_c, bar
Theory (CFM, ρ^4 model) [9, 10]	2696	246	283	2042	230	132
Simulation [12]	3932	353	1290	3120	277	534
Experiment [13]	2485	300	248	2280	190	161

term with $g_a > 0$ describes a uniform attraction influencing all particle pairs in the system, while the term with $g_r > 0$ is responsible for a short-range repulsion between two particles within the same cell. The stability of the interaction [17] is ensured by the inequality

$$g_r > g_a > 0. \quad (10)$$

Previous studies [7, 16] have established that the cell model under consideration admits an exact representation in the form of a single integral, whose asymptotic value in the thermodynamic limit is determined via Laplace's method. To achieve this, we need to find the maximum value $E_0(\bar{z}, \mu)$ of the function

$$E_0(z, \mu) = -(z - \beta\mu - \ln v^*)^2/2p_a + \ln K_0(z), \quad (11)$$

where $z = \bar{z}$ denotes the location of the global maximum.

The special function $K_0(z)$ is a representative of the family of functions

$$K_m(z) = \sum_{n=0}^{\infty} \frac{n^m}{n!} \exp\left(-\frac{fp_a}{2}n^2\right) \exp(zn), \quad (12)$$
$$m = 0, 1, 2, \dots.$$

These functions depend on the repulsion strength g_r and temperature through the definitions

$$f = \frac{g_r}{g_a}, \quad fp_a = p_r, \quad p_r = \beta g_r, \quad \beta = (k_B T)^{-1}. \quad (13)$$

The dimensionless volume $v^* = v/\Lambda^3$ is considered equal to v, as the de Broglie wavelength Λ is set to 1.

The chemical potential μ is given as a function of $\bar{z}$ by the relation

$$\beta\mu = \bar{z} - p_a \frac{K_1(\bar{z})}{K_0(\bar{z})} - \ln v^*, \quad (14)$$

where $p_a = \beta g_a$.

For the average particle density we have

$$\bar{n} = \frac{K_1(\bar{z})}{K_0(\bar{z})}. \quad (15)$$

The pressure P is obtained from the equation of state

$$Pv\beta_c = (\tau + 1)\left[\ln K_0(\bar{z}) - \frac{p_a}{2}\left(\frac{K_1(\bar{z})}{K_0(\bar{z})}\right)^2\right]. \quad (16)$$

The Curie–Weiss cell model exhibits a sequence of first-order phase transitions with certain critical temperatures [16]. In terms of the model parameters introduced just above, each critical temperature associated with the n-th critical point is given by

$$k_B T_c^{(n)} = g_a/p_{ac}^{(n)}. \quad (17)$$

Thus, the superscript n denotes the sequential number of the critical point in the series, starting from the *lowest* critical temperature $T_c^{(1)}$. The specific values of the critical temperatures $T_c^{(n)}$ depend on the chosen value of the Curie–Weiss attraction strength g_a. Since we are presently interested in the general behavior of the system, there is no need to assign a specific value to g_a. To simplify notation, we assume

$$T_c^{(1)} \equiv T_c \quad \text{and} \quad \beta_c^{(1)} \equiv \beta_c. \quad (18)$$

Table 2 presents our numerical results obtained for the first three critical points in the sequence, with the lowest critical temperatures. The cell volume v^* is set to $v^* = 5.0$. The interaction-strength ratio $f = g_r/g_a$ ranges from $f \gtrsim 1$ close to the marginal value $f = 1$ dictated by the stability condition (10) to $f = 10$ corresponding to the asymptotic regime $f \gg 1$. The specific case $f = 1$ is elaborated in [18]. Further discussion is deferred to the following section.

3.2. Influence of the attraction strength on critical parameters

This section analyzes the critical parameters of our cell model as presented in Table 2. We consider the critical values of pressure, temperature, density, and chemical potential. Our numerical results complement and extend the findings of [19].

The parameter $f = g_r/g_a$, introduced in (13), is inversely proportional to the attraction strength g_a and must satisfy the stability condition $f > 1$. Therefore, while fixing the repulsion strength g_r, we observe in Table 2 how the critical parameters change as the global Curie–Weiss attraction g_a decreases.

For each specific value of f, the critical temperature, critical density, pressure, and chemical potential all increase when transitioning to each subsequent critical point in the sequence. This increase, however, essentially slows down for the critical temperatures $T_c^{(n)}$. Specifically, for large f, such as $f > 3.0$, where repulsion significantly dominates attraction, the critical temperature for all first three phase transitions

Table 2. **Critical parameters for the first three critical points with the lowest critical temperatures $T_c^{(n)} = 1/p_{ac}^{(n)}$ at different values of $f = g_r/g_a$ and a fixed $v^* = 5.0$. The value β_c refers to $n = 1$ as in (18)**

f	n	$T_c^{(n)}$	$\bar{n}_c^{(n)}$	$P_c^{(n)}v\beta_c$	$\beta_c\mu_c^{(n)}$	f	n	$T_c^{(n)}$	$\bar{n}_c^{(n)}$	$P_c^{(n)}v\beta_c$	$\beta_c\mu_c^{(n)}$
1.00000001	1	0.2614	0.5355	0.2048	−1.6405	1.5	1	0.2513	0.5039	0.1944	−0.6184
	2	0.2841	1.5191	1.0261	−1.0098		2	0.2531	1.5014	2.8883	2.0604
	3	0.2988	2.5128	2.0406	−0.5921		3	0.2539	2.5007	7.6917	4.4578
1.0000001	1	0.2614	0.5355	0.2048	−1.6405	1.7	1	0.2506	0.5017	0.1937	−0.2143
	2	0.2841	1.5191	1.0261	−1.0098		2	0.2514	1.5006	3.6852	3.2708
	3	0.2988	2.5128	2.0406	−0.5921		3	0.2517	2.5003	10.0889	6.4708
1.000001	1	0.2614	0.5355	0.2048	−1.6405	2.0	1	0.2502	0.5005	0.1933	0.3887
	2	0.2841	1.5191	1.0261	−1.0098		2	0.2504	1.5002	4.8851	5.0787
	3	0.2988	2.5128	2.0406	−0.5921		3	0.2505	2.5001	13.6923	9.4817
1.00001	1	0.2614	0.5355	0.2048	−1.6405	2.5	1	0.2500	0.5001	0.1932	1.3902
	2	0.2841	1.5191	1.0262	−1.0097		2	0.2500	1.5000	6.8860	8.0828
	3	0.2988	2.5128	2.0407	−0.5920		3	0.2501	2.5000	19.6960	14.4877
1.0001	1	0.2614	0.5355	0.2048	−1.6403	3.0	1	0.2500	0.5000	0.1932	2.3905
	2	0.2841	1.5191	1.0264	−1.0092		2	0.2500	1.5000	8.8862	11.0835
	3	0.2987	2.5128	2.0415	−0.5911		3	0.2500	2.5000	25.6970	19.4889
1.001	1	0.2614	0.5353	0.2047	−1.6384	3.5	1	0.2500	0.5000	0.1931	3.3906
	2	0.2840	1.5190	1.0291	−1.0035		2	0.2500	1.5000	10.8863	14.0837
	3	0.2985	2.5127	2.0495	−0.5819		3	0.2500	2.5000	31.6972	24.4891
1.01	1	0.2609	0.5338	0.2042	−1.6200	4.0	1	0.2500	0.5000	0.1931	4.3906
	2	0.2822	1.5177	1.0562	−0.9467		2	0.2500	1.5000	12.8863	17.0837
	3	0.2955	2.5116	2.1314	−0.4905		3	0.2500	2.5000	37.6972	29.4892
1.05	1	0.2590	0.5277	0.2023	−1.5379	5.0	1	0.2500	0.5000	0.1931	6.3906
	2	0.2756	1.5134	1.1834	−0.6960		2	0.2500	1.5000	16.8863	23.0837
	3	0.2850	2.5082	2.5191	−0.0855		3	0.2500	2.5000	49.6972	39.4892
1.1	1	0.2571	0.5219	0.2004	−1.4351	7.0	1	0.2500	0.5000	0.1931	10.3906
	2	0.2695	1.5097	1.3541	−0.3854		2	0.2500	1.5000	24.8863	35.0837
	3	0.2760	2.5056	3.0420	0.4195		3	0.2500	2.5000	73.6972	59.4892
1.2	1	0.2546	0.5139	0.1977	−1.2298	10.0	1	0.2500	0.5000	0.1931	16.3906
	2	0.2619	1.5056	1.7194	0.2309		2	0.2500	1.5000	36.8863	53.0837
	3	0.2653	2.5030	4.1567	1.4292		3	0.2500	2.5000	109.6972	89.4892
1.3	1	0.2530	0.5090	0.1961	−1.0252						
	2	0.2575	1.5034	2.1018	0.8432						
	3	0.2594	2.5018	5.3174	2.4394						

asymptotically approaches the same value T_c. In this case, $g_a/k_{\mathrm{B}}T_c^{(n)} = p_{ac}^{(n)} \to 4.0$. This behavior is in agreement with analytical calculations performed in [18, Sec. 7]. This reference also contains a detailed treatment of another marginal case, $f = 1$.

We now analyze the behavior of the critical point parameters corresponding to the same index n for varying values of f. When $f \to 1$, all critical pa-

rameters for a given n tend to their limiting values (see Table 2). As the parameter f increases (corresponding to a decrease in attraction strength g_a), the reduced critical pressure $P_c^{(1)}v\beta_c$ shows a negligible decrease, while the pressures $P_c^{(n)}v\beta_c$ for subsequent critical points with $n = 2$ and $n = 3$ increase significantly. The critical temperatures $T_c^{(n)}$ gradually decrease, eventually becoming identical for large f
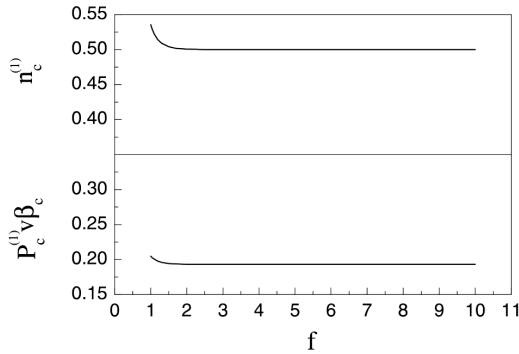
Fig. 1. Critical density $\bar{n}_c^{(1)}$ and critical pressure $P_c^{(1)} v \beta_c$ for the first critical point as a function of parameter f (with $v^* = 5.0$)
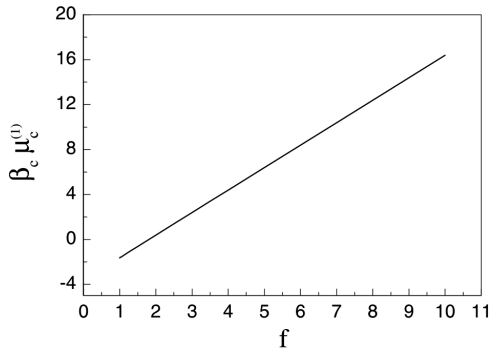

Fig. 2. Dependence of the critical chemical potential $\beta_c \mu_c^{(1)}$ at the first phase transition on the parameter f (with $v^* = 5.0$)

values as discussed in the previous paragraph. The critical density $\bar{n}_c^{(n)}$ also decreases negligibly with increasing f. Notably, regardless of the repulsion-to-attraction ratio f, the critical points consistently appear at approximately the same average densities: 0.5, 1.5, and 2.5. The slight decrease in critical density and pressure for the first critical point and their subsequent saturation for large f are illustrated in Fig. 1. The critical chemical potential values increase with f, and a typical picture is given in Fig. 2 for $n = 1$.

4. Conclusions

A characteristic feature of this study is the use of microscopic information about the interparticle interaction potential to evaluate the critical point parameters.

In the first part of the paper, we have investigated the influence of the attractive part of the interaction potential on the liquid-gas critical point in Morse flu-

ids. Numerical estimates are obtained using Morse potential parameters characteristic of alkali metals sodium and potassium. We converted the theoretical dimensionless critical point parameters into dimensional quantities often used in numerical and experimental studies. We show that a decrease in the width of the attractive part of the Morse potential leads to a reduction in both the critical temperature and pressure for both metals. Our results are in good agreement with existing data from other sources.

For the fluid cell model analyzed in the second part of this work, we investigated how the interparticle Curie–Weiss-type attraction strength influences the parameters for the first three critical points. We accomplished this by studying the results obtained with varying ratios $f = g_r/g_a$ of repulsion and attraction strenths.

For a specific value of f, the critical point parameters increase upon transitioning to each subsequent n. When attraction is significantly weaker than repulsion ($f > 3.0$), the critical temperature for all first three phase transitions becomes identical.

For varying f, we examined the critical points with the same index n, see Table 2. Thus, we found that, as the ratio f increases (i.e., attraction strength decreases), the critical temperatures $T_c^{(n)}$ gradually decrease, eventually becoming identical for large f. At the same time, we observed a slight decrease in the critical density and pressure for the first critical point, which then saturated. The critical density for $n = 2$ and $n = 3$ decrease negligibly with increasing f. Regardless of f, the critical points consistently appeared at approximately the same average densities. An increase in f also led to higher critical chemical potential in all considered cases.

Let us compare the effect of the attractive part of the Morse potential on the liquid-gas critical point with the effect of the attraction strength of the Curie–Weiss potential on the first critical point, considering the latter also as the liquid-gas critical point. The attractive components of these potentials have different functional forms. As mentioned above, narrowing the width of the attractive part of the Morse potential decreases the values of both the critical temperature and pressure. For the Curie–Weiss potential, a decrease in the attraction strenght g_a (or an increase in the parameter $f = g_r/g_a$) leads to an increase in the quantity $p_{ac}^{(1)}$ in expression (17) for the criti-

cal temperature [19], and therefore, to a decrease in $T_c^{(1)} \equiv T_c$. The critical pressure for the first phase transition point also decreases with an increase in f (see Table 2, $n = 1$). Thus, the consistent correlation is observed in how the attractive parts of two potentials of different types affect the behavior of the temperature and pressure at the liquid-gas critical point.

1. M.A. Anisimov. *Critical Phenomena in Liquids and Liquid Crystals* (Gordon and Breach, 1991), [ISBN: 9782881248061, 2881248063].

2. H. Behnejad, J.V. Sengers, M.A. Anisimov. *Thermodynamic Behaviour of Fluids near Critical Points.* In: *Applied Thermodynamics of Fluids.* Edited by A.R.H. Goodwin, J.V. Sengers, C.J. Peters (Royal Society of Chemistry, 2010).

3. J.-P. Hansen, I.R. McDonald. *Theory of Simple Liquids: With Applications to Soft Matter* (Academic Press, 2013) [ISBN: 9780123870322].

4. L.F. Vega. Perspectives on molecular modeling of supercritical fluids: From equations of state to molecular simulations. Recent advances, remaining challenges and opportunities. *J. Supercrit. Fluids* **134**, 41 (2018).

5. A. Oleinikova, L. Bulavin, V. Pipich. Critical anomaly of shear viscosity in a mixture with an ionic impurity. *Chem. Phys. Lett.* **278**, 121 (1997).

6. Y. Kozitsky, M. Kozlovskii, O. Dobush. *Phase Transitions in a Continuum Curie-Weiss System: A Quantitative Analysis.* In: *Modern Problems of Molecular Physics.* Edited by L.A. Bulavin, A.V. Chalyi (Springer, 2018).

7. Yu.V. Kozitsky, M.P. Kozlovskii, O.A. Dobush. A phase transition in a Curie-Weiss system with binary interactions. *Condens. Matter Phys.* **23**, 23502 (2020).

8. P.M. Morse. Diatomic molecules according to the wave mechanics. II. Vibrational levels. *Phys. Rev.* **34**, 57 (1929).

9. M.P. Kozlovskii, I.V. Pylyuk, O.A. Dobush. The equation of state of a cell fluid model in the supercritical region. *Condens. Matter Phys.* **21**, 43502 (2018).

10. I.V. Pylyuk. Fluid critical behavior at liquid–gas phase transition: Analytic method for microscopic description. *J. Mol. Liq.* **310**, 112933 (2020).

11. I.V. Pylyuk, M.P. Kozlovskii, O.A. Dobush. Analytic calculation of the critical temperature and estimation of the critical region size for a fluid model. *Ukr. J. Phys.* **68**, 601 (2023).

12. J.K. Singh, J. Adhikari, S.K. Kwak. Vapor–liquid phase coexistence curves for Morse fluids. *Fluid Phase Equilib.* **248**, 1 (2006).

13. F. Hensel. Critical behaviour of metallic liquids. *J. Phys.: Condens. Matter* **2**, SA33 (1990).

14. R.C. Lincoln, K.M. Koliwad, P.B. Ghate. Morse-potential evaluation of second- and third-order elastic constants of some cubic metals. *Phys. Rev.* **157**, 463 (1967).

15. H. Okumura, F. Yonezawa. Liquid-vapor coexistence curves of several interatomic model potentials. *J. Chem. Phys.* **113**, 9162 (2000).

16. M.P. Kozlovskii, O.A. Dobush. Phase behavior of a cell model with Curie–Weiss interaction. *J. Mol. Liq.* **353**, 118843 (2022).

17. D. Ruelle. Superstable interactions in classical statistical mechanics. *Commun. Math. Phys.* **18**, 127 (1970).

18. O.A. Dobush, M.A. Shpot. A new special function related to a discrete Gauss–Poisson distribution and some physics of the cell model with Curie-Weiss interactions. Preprint arXiv: 2412.05428 [cond-mat.stat.mech, math.CA], 20 p. (2024).

19. O.A. Dobush, M.P. Kozlovskii, I.V. Pylyuk, Yu.O. Plevachuk. Influence of microscopic parameters on phase behavior of a cell model with Curie–Weiss interaction. Preprint arXiv: 2505.14456 [cond-mat.stat.mech], 11 p. (2025).

І.В. Пилюк, О.А. Добуш,
М.П. Козловський, Р.В. Романік, М.А. Шпот

ВПЛИВ ПРИТЯГАЛЬНИХ ЧАСТИН ПОТЕНЦІАЛІВ ВЗАЄМОДІЇ НА ПАРАМЕТРИ КРИТИЧНИХ ТОЧОК

Досліджується вплив мікроскопічних деталей міжчастинкових потенціалів на макроскопічні параметри критичних точок. Наші аналітичні розрахунки базуються на комірковій моделі для неперервних багаточастинкових систем. Розглянуто два типи парних взаємодій, що описуються потенціалом Морзе та потенціалом типу Кюрі–Вейса. Для плинів Морзе представлено числові результати, отримані з використанням мікроскопічних параметрів, що відповідають лужним металам натрію (Na) та калію (K). Обчислені безрозмірні параметри критичних точок для рідких Na та K, виражені в розмірних одиницях, дають змогу безпосередньо порівнювати їх з наявними експериментальними та модельними даними. Для коміркової моделі Кюрі–Вейса з конкуруючими взаємодіями, яка демонструє послідовність фазових переходів першого роду, досліджено критичні параметри для перших трьох критичних точок. Отримані результати проаналізовано шляхом зміни притягальної частини потенціалу Морзе та сили притягання потенціалу типу Кюрі–Вейса, що дало змогу з'ясувати, як ці мікроскопічні характеристики змінюють координати критичних точок.

К л ю ч о в і с л о в а: потенціал Морзе, потенціал типу Кюрі-Вейса, сила притягання, параметри критичної точки, фазові переходи.